The Electrochemical Corrosion of Bulk Nanocrystalline Ingot Iron in Acidic Sulfate Solution

ARTICLE *in* THE JOURNAL OF PHYSICAL CHEMISTRY B · FEBRUARY 2006

Impact Factor: 3.3 · DOI: 10.1021/jp0538971 · Source: PubMed

6 AUTHORS, INCLUDING:

S.G. Wang
Chinese Academy of Sciences
34 PUBLICATIONS **476** CITATIONS
SEE PROFILE

Fiona Hong Wang
Chinese Academy of Sciences
37 PUBLICATIONS **919** CITATIONS
SEE PROFILE

The Electrochemical Corrosion of Bulk Nanocrystalline Ingot Iron in Acidic Sulfate Solution

S. G. Wang,*,† C. B. Shen,‡,§ K. Long,‡ T. Zhang,‡ F. H. Wang,‡ and Z. D. Zhang†

Shenyang National Laboratory for Materials Science, Institute of Metal Research, and International Centre for Materials Physics, Chinese Academy of Sciences, 72 Wenhua Road, 110016, Shenyang, P. R. China, State Key Laboratory for Corrosion and Protection, Institute of Metal Research, Chinese Academy Sciences, 62 Wencui Road, 110016, Shenyang, P. R. China, and Department of Materials Science and Engineering, Dalian Jiaotong University, 793 Huanghe Road, 116028, Dalian, P. R. China

Received: July 15, 2005; In Final Form: September 29, 2005

The corrosion properties of bulk nanocrystalline ingot iron (BNII) fabricated from conventional polycrystalline ingot iron (CPII) by severe rolling were investigated by means of immersion test, potentiodynamic polarization (PDP), electrochemical impedance spectroscopy (EIS) tests, and scanning electron microscopy (SEM) observation. These experimental results indicate that BNII possesses excellent corrosion resistance in comparison with CPII in acidic sulfate solution at room temperature. It may mainly result from different surface microstructures between CPII and BNII. However, the corrosion resistance of nanocrystalline materials is usually degraded because of their metastable microstructure nature, and the residual stress in nanocrystalline materials also can result in degradation of corrosion resistance according to the traditional point of view.

1. Introduction

Nanocrystalline materials exhibit some improved properties over their coarse-grained counterparts.[1] The characterization of the corrosion behavior of nanocrystalline materials is important for both prospective engineering applications and better understanding of their fundamental properties.[2] However, the corrosion behaviors of bulk nanocrystalline (NC) materials have been scarcely studied to date. Their corrosion resistance was found to be usually degraded because of their metastable microstructure nature.[3−8] The mechanically alloyed nanocrystalline Co−Cu alloys showed corrosion rates higher than those of as-cast alloys.[9] The corrosion rates of nanocrystallized surface fabricated on low carbon steel by using ultrasonic shot peening were also higher than those of counterparts.[3] The significant degradation of corrosion resistance of NC Ni−P in sulfuric acid was also reported for grain sizes of 8.4 and 22.6 nm.[4] Moreover, the average dissolution rate of NC Ni was higher than that of conventional Ni.[5] The corrosion behavior of ultrafine-grained (UFG) Cu produced by equal channel angular extrusion (ECAE) and polycrystalline Cu[6] was investigated by Livingston etchant.[7] The steady-state anodic current density of UFG Cu was higher than that of conventional polycrystalline copper counterparts.

To the authors' knowledge, there have been no reports on electrochemical corrosion behavior of BNII in acidic sulfate solution so far. In this work, the electrochemical corrosion behavior of BNII and CPII was investigated by means of immersion test, potentiodynamic polarization (PDP), electrochemical impedance spectroscopy (EIS) tests, and scanning electron microscopy (SEM) observation. The interesting and surprising results of electrochemical corrosion behavior for BNII were obtained.

2. Experimental Section

The materials used in this study were CPII and BNII, and BNII was prepared from CPII by severe rolling technique. In the present work, BNII was not treated with any methods including heat treatment after severe rolling. The details of the severe rolling technique and the microstructure characterization of CPII and BNII were described in our previous work.[10] All corrosion tests were carried out in 0.05 M H_2SO_4 + 0.25 M Na_2SO_4 solution at room temperature. The corrosion rates of BNII and CPII were inspected by CMB-1510 Portable Corrosion Rate Measurement Instrument in immersion test. This instrument was produced by the Corrosion Inspecting Center in the Institute of Metal Research, Chinese Academy of Sciences, Shenyang, China.[11] The specimen surfaces of BNII and CPII for PDP, corrosion rates, and EIS tests were mechanically polished up to 0.6 μm SiC paper and ultrasonically cleaned. Subsequently, they were degreased in acetone. These treatments ensured good reproducibility of electrochemical measurements. The working electrode area was 10 × 10 mm^2. Potentiodynamic polarization tests were conducted by using an EG&G model 273 potentiostat with a standard corrosion cell containing graphite counter electrodes and saturated calomel electrode (SCE). Prior to PDP tests, all specimens were cathodically polarized at a potential of −1350 mV_{SCE} for 15 min in order to remove any surface film that may have formed on the specimen. The applied potential was then removed, and the system was monitored until a steady-state open-circuit potential (E_{corr}) was reached. The potential was scanned from −300 to 1500 mV vs E_{corr} at a scan rate of 0.33 mV/sec. Some electrochemical parameters related to PDP, E_{corr}, corrosion current I_{corr}, anodic Tafel slope b_a, and cathodic Tafel slope b_c of BNII and CPII were provided after analysis by the POWERCORR software. The passive potential

* Corresponding author. Fax: 86-24-23891320. E-mail: sgwang@imr.ac.cn.

† Shenyang National Laboratory for Materials Science, Institute of Metal Research, and International Centre for Materials Physics, Chinese Academy of Sciences.

‡ State Key Laboratory for Corrosion and Protection, Institute of Metal Research, Chinese Academy Sciences.

§ Dalian Jiaotong University.

10.1021/jp0538971 CCC: $33.50
Published on Web 12/10/2005

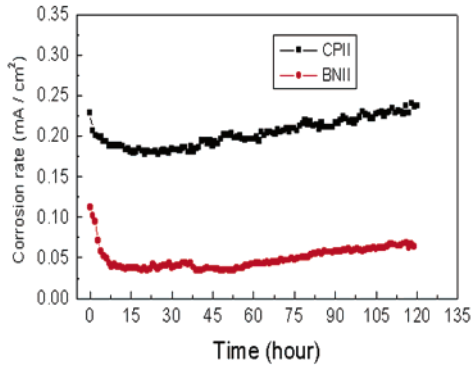

Figure 1. Corrosion rates of BNII and CPII in 0.05 M H_2SO_4 + 0.25 M Na_2SO_4 solution.

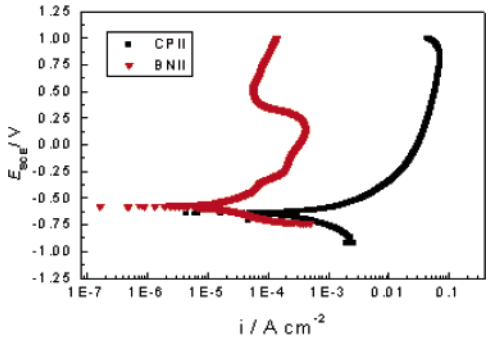

Figure 2. PDP curves of BNII and CPII in 0.05 M H_2SO_4 + 0.25 M Na_2SO_4 solution.

E_p of BNII was also measured. EIS measurements were carried out on an EG&G PARC Parstat 2263 at E_{corr}, and the amplitude of AC sine wave was 10 mV. The applied frequency ranged from 10^5 to 10^{-2} Hz. The impedance data, such as the resistance of solution R_s, the resistance of charge transfer R_t, and the double-layer capacitance of the interface C_{dl}, were analyzed by Zsimpwin software. The Nyquist and Bode plots of BNII and CPII were drawn. The morphologies of corrosion surfaces for BNII and CPII after polarization tests were analyzed by Philip XL30 scanning electrode microscope (SEM).

3. Results and Discussion

3.1. Immersion Test. The corrosion rates of BNII and CPII in situ measurement are shown in Figure 1. The measurement interval was 120 h. The corrosion rates of BNII and CPII were almost invariable during the measurement interval, as revealed by Figure 1. This is easy to understand for CPII, because the microstructure of CPII is isotropic. However, the microstructure of BNII is anisotropic, because BNII suffered from severe rolling. We would draw a conclusion that the microstructure of the rolled plane on the surface is the same as that inside for BNII. This is an advantage of BNII in corrosion properties. From Figure 1, the corrosion rate of BNII is only about one-fourth that of CPII during the whole immersion interval, which means that BNII produces an excellent corrosion resistance in comparison with CPII.

3.2. PDP Test. PDP curves of BNII and CPII are shown in Figure 2. Some notable differences in corrosion behavior and electrochemical parameters are evident. (1) It should be noted that the corrosion current densities of both anode and cathode of BNII are extremely lower than those of CPII. (2) The whole PDP curve of BNII is on the top left-hand side of the PDP curve of CPII over the entire potential range. (3) BNII displays the active−passive−transpassive−active behavior, but CPII only displays the active behavior without passivation. The potential of passivation of BNII E_p is about 235 mV (SCE). E_{corr} of BNII is 70 mV more positive than that of CPII. I_{corr} of BNII is only $^1/_{20}$ that of CPII. The electrochemical parameters, I_{corr}, E_{cor}, b_a, and b_c of BNII and CPII, and E_p of BNII are listed in Table 1. b_a of BNII is about 1.3 times that of CPII and b_c of CPII is 1.69 times that of BNII from Table 1. Figure 2 also shows that the dissolution rates of BNII are lower than those of CPII. Figure 2 indicates that the corrosion resistance of BNII is better than that of CPII.

TABLE 1: Electrochemical Parameters of BNII and CPII in 0.05 M H_2SO_4 + 0.25 M Na_2SO_4 at Room Temperature

sample	b_a (mV)	b_c (mV)	I_{corr} (A cm^{-2})	E_{corr} (mV)	E_p (mV)	R_s (ohm cm^2)	C_{dl} (μF cm^{-2})	R_t (ohm cm^2)
BNII	347.9	198.6	2.415×10^{-5}	−576	235	16.12	7.56	1040.27
CPII	151.2	337.2	4.831×10^{-4}	−646		16.91	46.7	96.81

3.3. Morphologies of Corrosion Surface of CPII and BNII. Figure 3 represents the morphologies of corrosion surfaces of CPII and BNII during polarization tests at 400 mV (SCE). Figure 3a is the morphology of the corrosion surface of CPII, while Figure 3b is the morphology of the corrosion surface of BNII. The two morphologies were observed with the same resolution. Figure 3c is the morphology of the corrosion surface of BNII at higher resolution. For BNII, there was not obvious selected corrosion (such as intergranular corrosion and corrosion along certain plane) from Figure 3b and 3c. CPII suffered from intensively intergranular corrosion, and the corrosion inside CPII grain was uniform. This results in the whole crystalline grain coming off the corrosion surface in the corrosion process, according to Figure 3a. It causes an enhanced corrosion rate for CPII. However, the corrosion surface of BNII is relatively uniform without large bulk iron coming off the corrosion surface during the corrosion process. This indicates that the corrosion of BNII is more uniform than that of CPII as seen from Figure 3a and b. Figure 3 demonstrates that CPII is more liable become corroded than BNII.

3.4. EIS and Bode Plots of BNII and CPII. Figure 4 gives EIS of BNII and CPII. Figure 5 is its equivalent circuit. The Bode plots of BNII and CPII are shown as Figure 6. In Figure 4, the two semicircles with centers below the real axis indicate that the charge-transfer process controls the dissolution of iron for both BNII and CPII and that the dissolution of BNII and CPII is an electrochemical control process. The values of R_t and C_{dl} for BNII and CPII are listed in Table 1. R_t of BNII is about ten times larger than that of CPII. R_t, which corresponds to the low-frequency limit of the magnitude of the impedance, is inversely proportional to the corrosion rate. From Figure 6, δ_{max} (the maximum phase angle) and ω^{δ}_{max} (the frequency corresponding to the maximum phase angle) of BNII are 76.2° and 1026 Hz, respectively. δ_{max} and ω^{δ}_{max} of CPII are 46.6° and 580 Hz, respectively. C_{dl} of BNII is about five times smaller than that of CPII. The lower value of C_{dl} implies the formation of a thicker protective film on the electrode surface for BNII, which can make the following two reactions occur with lower reaction rates than those for CPII:

$$Fe \leftrightarrow Fe^{2+} + 2e \quad (1)$$

$$Fe^{2+} + 2e + 2H_2O \leftrightarrow Fe + nH_2O \quad (2)$$

Therefore, the corrosion resistance of BNII is enhanced. EIS measurement as shown in Figure 4 indicates that the corrosion rate of BNII is lower than that of CPII. This result is consistent

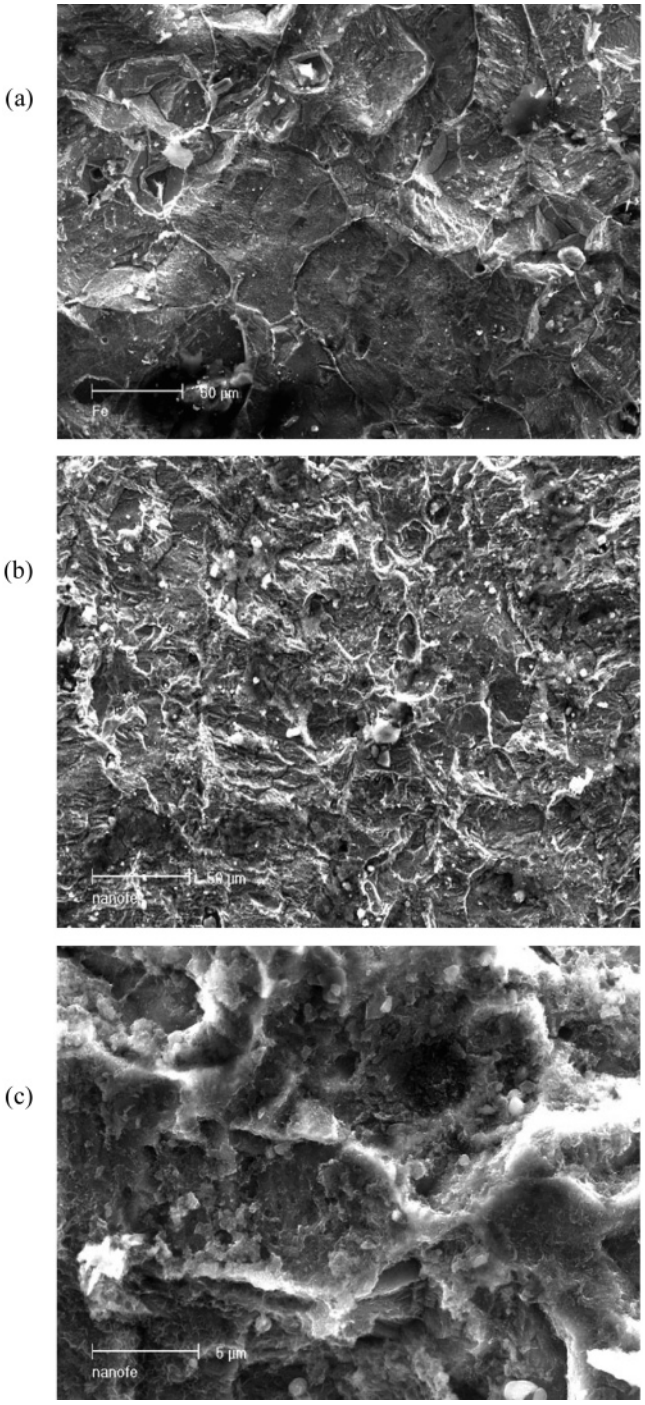

Figure 3. Morphologies of CPII and BNII corrosion surfaces. (a) CPII; (b, c) BNII.

with corrosion rate in situ measurement, PDP tests, and the observation of the corrosive surface for BNII and CPII.

3.5. Discussion. Figures 1−5 indicate that the corrosion resistance of BNII is enhanced in comparison with that of CPII by corrosion rate in situ measurement, PDP test, and EIS measurement. From a traditional metallurgical viewpoint, corrosion is particularly associated with structural inhomogeneity resulting from precipitations and other lattice defects. One of the most dangerous localized types of damage is intergranular corrosion associated with grain boundaries[12,13] Intercrystalline constituents, grain boundaries, and triple junctions are considered to be distinct defects that provide active dissolution sites.[8] The overpotentials of anode and cathode is the main dynamic factor

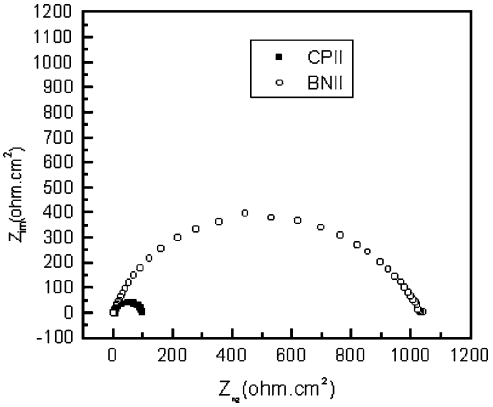

Figure 4. Nyquist plots of BNII and CPII.

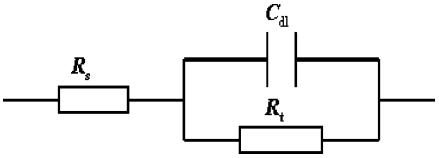

Figure 5. Quivalent circuit for EIS spectrum measurement.

for determining corrosion rate. The anodic overpotential η_a and cathodic overpotential η_c for BNII and CPII are

$$\eta_a = b_a \log\left(\frac{i_a}{i_{corr}}\right) \tag{3}$$

$$\eta_c = b_c \log\left(\frac{i_c}{i_{corr}}\right) \tag{4}$$

The anodic reaction rate is inversely proportional to η_a. The cathodic reaction rate is directly proportional to η_c. Figure 6 shows the anodic and cathodic overpotentials versus the current density for BNII and CPII according to eqs 3 and 4. From Figure 6, η_a of BNII is more positive than that of CPII, and η_c of the former is more negative than that of the latter at the same current density. Figure 6 means that the anodic and cathodic reaction rates of BNII are lower than those of CPII. This is one of the electrochemical factors resulting in the enhanced corrosion resistance for BNII. In addition, the polarization of CPII was only involved in active polarization. However, the polarization of BNII includes active polarization and resistance polarization from Figure 2.

In acidic sulfate solutions, which are free of oxygen, other oxidizing agents, and surface substances, the anodic activation dissolution of pure iron processes by one of two different reaction mechanisms

$$Fe + H_2O \leftrightarrow (FeOH)_{ads} \tag{5a}$$

$$(FeOH)_{ads} \leftrightarrow Fe(OH^-)_{ads} + H^+ \tag{5b}$$

$$Fe(OH^-)_{ads} \leftrightarrow Fe(OH)_{ads} + e \tag{5c}$$

$$Fe + H_2O \leftrightarrow Fe(OH)_{ads} + H + e \tag{5}$$

Consecutive mechanism[14]

$$Fe(OH)_{ads} \rightarrow FeOH^+ + \quad \text{(rate-determining step)} \tag{6}$$

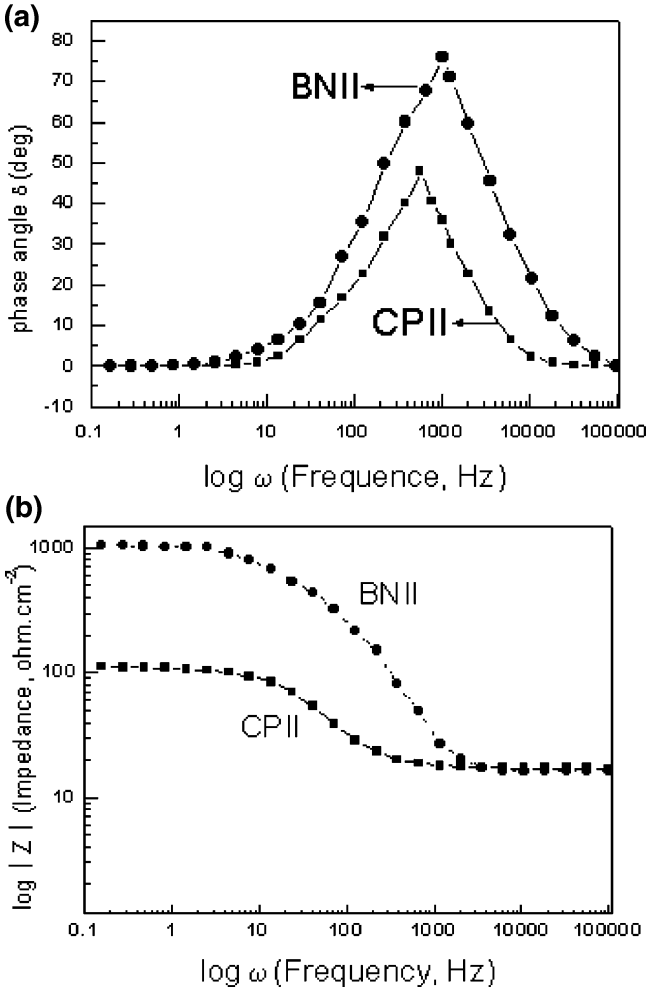

Figure 6. Frequency dependence of phase angle δ (a) and impedance $|Z|$ (b).

Catalyzed mechanism[15]

$$\mathrm{Fe} + \mathrm{Fe(OH)_{ads}} \leftrightarrow \mathrm{Fe(FeOH)} \quad (7)$$

$$\mathrm{Fe(FeOH)} + \mathrm{OH^-} \rightarrow \mathrm{FeOH^+} + \mathrm{(FeOH)_{ads}} + 2\mathrm{e} \quad \text{(rate-determining)} \quad (8)$$

$$\mathrm{FeOH^+} + \mathrm{H^+} \leftrightarrow \mathrm{Fe^{2+}(aq)} + \mathrm{H_2O} \quad (9)$$

In the consecutive mechanism, $(FeOH)_{ads}$ acts as a reaction intermediate rather than a catalyst. In the catalyzed mechanism, $(FeOH)_{ads}$ acts as a catalyst. The cathodic reaction is a hydrogen depolarization process; the general reaction scheme for the hydrogen evolution reaction is given by eqs 10−12

$$\mathrm{H^+} + \mathrm{e} \rightarrow \mathrm{H_{ads}} \quad (10)$$

$$\mathrm{H_{ads}} + \mathrm{H^+} + \mathrm{e} \rightarrow 2\mathrm{H_{ads}} \quad (11)$$

$$2\mathrm{H_{ads}} \rightarrow \mathrm{H_2} \quad (12)$$

A comparative study has been made of the electrochemical behavior of the active iron electrode in noninhibiting media; many previous investigations have led to a variety of conflicting results. The kinetics of dissolution of active iron in acidic sulfate solutions is controversial. Values of $b_{a,Fe}$ varying between 30 and 100 have been reported according to experimental results and theoretical analysis based on the two reaction mechanisms.[16−20] First- or second-order dependence of the anodic reaction upon the hydroxyl ion activity has been suggested. These results refer to different experimental conditions, degree of purity, surface preparation, and different polarization methods. Eldakar[21] has suggested that the change of Tafel slope for steel in H_2SO_4 is due to the difference in carbon content in steel. They pointed out that the value of anodic Tafel slopes increases with increasing carbon content. The influences of pH, potential, and C content on the steady-state dissolution of iron have been investigated in H_2-saturated sulfate solutions. The Tafel slope b_a was 60 mV/decade, which was independent of pH or C content.[18] The polarization resistance R_p is defined as the tangent of a polarization curve at E_{corr}

$$R_p = \left(\frac{dE}{di}\right)_{E=E_{corr}} \quad (13)$$

In the case of simple, charge-transfer-controlled reactions, the corrosion current density, I_{corr}, is related to R_p by the Stern−Geary equation[22,23]

$$R_p = \frac{b_a.b_c}{2.3(b_a + b_c)}\frac{1}{I_{corr}} \quad (14)$$

According to eq 14, R_p values of BNII and CPII are 2273.17 ohm cm^2 and 93.83 ohm cm^2, respectively. R_p of CPII agrees with EIS measurement within error. However, R_p of BNII obtained from eq 14 is about 1.2 times larger than R_t. The important result of this analysis is that the transfer resistance R_t is smaller than the polarization resistance R_p for BNII. The present results of Tafel slope b_a and b_c, transfer resistance R_t, and polarization resistance R_p for BNII are very different from previous experimental results and theoretical analysis, which means that the possible new mechanism controls the corrosion process for BNII.

The enhanced dissolution rates of NC Ni−P in comparison with conventional polycrystalline nickel in 0.1 M sulfuric acid were attributed to the metastability and considerable volume fractions of grain boundaries and triple junctions.[4] The corrosion rates of mechanically alloyed Co−Cu alloys were higher than those in as-cast alloys, which was due to the high value of stored energy presented in mechanical alloying as a result of the severe plastic deformation during ball milling.[9] For UFG Cu[7] and NC Ni (99.99%) produced by electrodeposition,[5] the average dissolution rates were higher than those of conventional polycrystalline materials because of the unique structure of NC materials, which contained considerable volume fractions of grain boundaries and tripe junctions. High internal stress within the grains may also facilitate general matrix corrosion in NC states. Therefore, the acceleration of corrosion was not surprising.[7]

The texture structure of ingot iron is along ⟨111⟩ (123), ⟨111⟩ (112), ⟨111⟩ (110) or their combination after rolling, which depends on the degree of deformation.[24] According to our previous work,[10] the texture structure of BNII is ⟨111⟩ (110), The X- ray diffraction patterns of BNII and CPII were shown as Figure 7.[10] It is well-known that the polycrystalline iron surface is inhomogeneous and contains discontinuities such as grain boundaries, atomic step, and so forth. It is very difficult to estimate the degree of surface inhomogeneity. The effect of plastic deformation on metal corrosion has been investigated extensively for iron and steel.[25−30] According to classical points of view, the residual stress in materials can result in degradation of corrosion resistance[27−30] and became more pronounced with increasing deformation.[25,28] The increased corrosion rate was

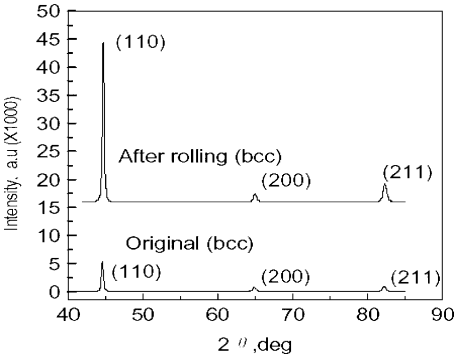

Figure 7. X-ray diffraction patterns of BNII (after rolling) and CPII (original).

due to an increase in the rate of anodic dissolution, and the hydrogen evolution was only negligibly affected by plastic deformation.[25] Hydrogen evolution was independent of plastic deformation, as expected, because the reduction of hydrogen ions did not depend on metallic bond energies. Plastic deformation had an effect on anodic and cathodic Tafel constants of zone-refined iron, but shifted polarization curves to higher current densities.[25] Plastic deformation increased the number and/or the activity of dislocations on the surface of iron. Corrosion tended to become more localized as plastic deformation increased. The disarray in the atomic structure brought about by plastic deformation was likely to facilitate detachment of the atom from metallic phase and its passage into the liquid.[27] Plastic deformation increased corrosion, the effect of strain being one of rupturing oxide films on the metal surface or decreasing ohmic resistance of microcells such as by breaking up the grain structure.[29] In general, etchability of interfaces immersed in electrolytic solutions was closely related to their internal energies: the higher the internal energy, the greater corrosion degradation of the interface region.[12,13,31] Since a large portion of the elastic energy was stored in such heavily deformed materials, it was natural to expect a higher dissolution rate in the NC state, compared with the coarse-grained samples. The disarrayed lattice or increased active sites for dissolution of iron were the cause of increased corrosion following plastic deformation.

It is obvious that the present data do not support the previous views shown above. It should be noticed that plastic deformation increases the internal energy and residual stress of BNII and that the volume fractions of grain boundary and triple junction of BNII are also higher than those of CPII. However, the results of the present work are in contradiction to those of previous experiments.[3−7,25−30] It is surprising that the three factors do not enhance the reaction rates of both anode and cathode. BNII produces pronounced corrosion resistance in 0.05 M H_2SO_4 + 0.25 M Na_2SO_4 solution at room temperature. Therefore, we have to think that the three factors are not sufficient conditions for enhancing corrosion rates of nanocrystalline materials; corrosion properties of nanocrystalline materials depend on the actual microstructure of nanocrystalline materials prepared by different techniques.

The main reason for enhanced corrosion properties of BNII in comparison with CPII may be related to the difference between their microstructures.[32,33] The reasons may be attributed to the following: (1) The preferential orientation ⟨111⟩ (110) was dominant, and disordered orientation disappeared for BNII according to our previous work.[10] There were a smaller number of dislocations in the rolled surface for BNII than that for CPII, resulting in the decrease of corrosion rates for both anode and cathode as shown in Figure 2. It should be noticed that the

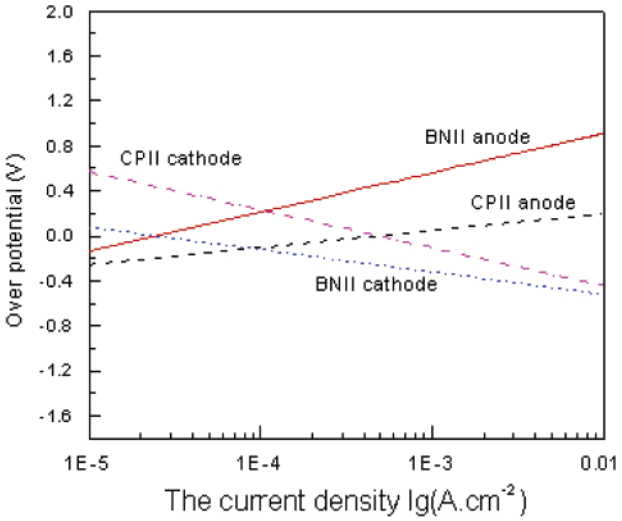

Figure 8. Overpotentials of anode and cathode for BNII and CPII.

binding energy (or surface energy) of atoms in the (110) plane is the minimum for bcc metals,[34] in which the activity of atoms was inhibited. From Figure 7, the surface energy of the rolled surface for BNII should be the surface energy of the crystalline plane (110). The surface energy (γ) of a certain crystalline plane of metal can be shown as[34]

$$\gamma = \frac{Jt}{2r_0^2}\frac{n_A}{D(n_A)}\mathrm{DBB} \tag{15}$$

DBB denotes the densities of broken bonds of certain crystalline plane. r_0 is the crystalline constant of metal. n_A and $D(n_A)$ are the parameters associated with the metal atom. J is

$$J = \frac{75}{m - 0.36\epsilon} \tag{16}$$

where m and ϵ are parameters of metal bonds. t is the bond-forming power

$$t = \sqrt{\alpha} + \sqrt{3\beta} + \sqrt{5\lambda} + \sqrt{7\phi} \tag{17}$$

α, β, λ, and φ are the ingredients of s, p, d, and f orbitals in the hybrid bond orbital, respectively. According to eq 15, the surface energy of BNII ((110) plane) is 2.05 J/m^2.[34] For CPII, the orientation of the crystalline plane on the surface is stochastic. Therefore, the surface energy of CPII is the average value of surface energy. It is 2.36 J/m^2.[35] (2) The little difference of internal energy between atoms inside the grain and those around the grain boundary also results in the decrease in corrosion rates for both anode and cathode and uniform corrosion for BNII as shown in Figure 2. (3) The difference in surface microstructure between BNII and CPII results in anodic (or cathodic) overpotential of BNII being more positive (or negative) than that of CPII (Figure 8), which causes smaller reaction rates of both anode and cathode for BNII. In fact, the corrosion properties of nanostructured materials depended strongly on the preparation technique, thermal history, and material purity, as well as other factors.[6]

4. Conclusion

The severe plastic deformation results in the texture structure ⟨111⟩ (110) (preferential crystalline orientation), which can enhance corrosion resistance of ingot iron. A large volume fraction of nonequilibrium grain boundaries and high residual

stress inside the grain for BNII does not degrade corrosion resistance. The differences of the surface microstructure between BNII and CPII result in the difference of the overpotential between BNII and CPII, which are largely accountable for the disparity in some corrosion behaviors between them in the view of electrochemistry. The two advantages of BNII in corrosion properties are the enhanced corrosion resistance and homogeneous corrosion in comparison with conventional polycrystalline ingot iron in acidic sulfate solution.

Acknowledgment. We acknowledge the financial support from the National Natural Science Foundation under the contracts no. 50501023 and 10274087.

References and Notes

(1) Gleiter, H. *Prog. Mater. Sci.* **1989**, *33*, 223.
(2) Valiev, R. Z.; Krasilnikov, N. A.; Tsenev, N. K. *Mater. Sci. Eng., A* **1991**, *35*, 137.
(3) Li, Y.; Wang, F. H.; Liu, G. *Corrosion* **2004**, *60*, 891.
(4) Rofagha, R.; Erb, U.; Ostander, D.; Palumbo, G.; Aust, K. T. *Nanostruct. Mater.* **1993**, *2*, 1.
(5) Rofagha, R.; Langer, R.; El-Sherik, A. M.; Erb, U.; Palumbo, G.; Aust, K. T. *Scr. Metall.* **1991**, *25*, 2867.
(6) Valiev, R. Z.; Islamgaliev, R. K.; Alexandrov, I. V. *Prog. Mater. Sci.* **2000**, *45*, 103.
(7) Vinogradov, A.; Mimaki, T.; Hashimoto, S.; Vailev, R. Z. *Scr. Mater.* **1999**, *41*, 319.
(8) Palumbo, G. Ph.D. Thesis. University of Toronto, 1989.
(9) Lopez-Hirata, V. M.; Arce-Estrada, E. M. *Electrochim. Acta* **1997**, *42*, 61.
(10) Wang, S. G.; Shen, C. B.; Long, K.; Yang, H. Y.; Wang, F. H.; Zhang, Z. D. J. *Phys. Chem. B* **2005**, *109*, 2499.
(11) Li, Y.; Qu, L.; Wang, F. H. *Corros. Sci.* **2003**, *45*, 1367.
(12) Aust, K. T.; Erb, U.; Palumbo, G. *Mater. Sci. Eng., A* **1994**, *176*, 329.
(13) Yamashita, M.; Timaki, T.; Hashimoto, S.; Miura, S. *Philos. Mag. A* **1991**, *63*, 707.
(14) Bockris, J. O'M.; Drazic, D.; Despic, A. R. *Electrochim. Acta* **1961**, *4*, 325.
(15) Heusler, K. E. *Z. Elektrochem.* **1958**, *62*, 582.
(16) Lorenz, W. J.; Eichkorn, G. *Ber. Bunsen-Ges.* **1966**, *70*, 99.
(17) Eichkorn, G.; Lorenz, W. J.; Albert, L.; Fischer, H. *Electrochim. Acta* **1968**, *13*, 183.
(18) Abdul Azim, A. A.; Sanad, S. H. *Electrochim. Acta* **1972**, *17*, 1699.
(19) Makrides, A. C. *J. Electrochem. Soc.* **1960**, *107*, 869.
(20) Cao, C. N. *The mechanism of corrosion electrochemistry*; Chemical Industry Press: Beijing, China, 2004; p 74.
(21) Eldakar, N.; Nobe, K. *Corrosion* **1981**, *37*, 271.
(22) Stern, M.; Geary, A. L. *J. Electrochem. Soc.* **1955**, *102*, 609.
(23) Stern, M.; Geary, A. L. *J. Electrochem. Soc.* **1957**, *104*, 56.
(24) *The encyclopedia of materials science and technology*; Li, C. G., Ed.; China Encyclopedia Press: Beijing, China, 1995; p 427.
(25) Greene, N. D.; Slatzman, G. A. *Corrosion* **1964**, *20*, 293t.
(26) Edwards, C. A.; Phillips, D. L.; Thomas, D. E. *J. Iron Steel Inst., London* **1938**, *137*, 223P.
(27) Tammann, G.; Neubert, F. *Z. Anorg. Chem.* **1932**, *207*, 87.
(28) Evans, U. R. *Corrosion and Oxidation of Metals*; Edward Arnold Ltd.: London, 1960; p 386.
(29) Zaretski, E. M. *J. Appl. Chem. (Leningrad)* **1951**, *24*, 521.
(30) Stern, M. *J. Electrochem. Soc.* **1955**, *102*, 663.
(31) Mimaki, T.; Yamashita, M.; Hashimoto, S.; Miura, S. *Mater. Forum* **1990**, *14*, 9.
(32) Schwerckert, H.; Lorentz, W. J.; Friedburg, H. *J. Electrochem. Soc.* **1980**, *127*, 1693.
(33) Li, P.; Tan, T. C.; Lee, J. Y. *Corros. Sci.* **1996**, *38*, 1935.
(34) Wang, S. G.; Tian, E. K.; Lung, C. W. *J. Phys. Chem. Solids* **2000**, *60*, 1295.
(35) Tyson, W. R.; Miller, W. A. *Surf. Sci.* **1977**, *62*, 267.